Synthesis of calcium oxalate trihydrate: New data by vibrationalspectroscopy and synchrotron X-ray diffraction

Claudia Conti[a], Marco Casati[a,b], Chiara Colombo[a], Elena Possenti[a], Marco Realini[a], G. Diego Gatta[c,d],Marco Merlini[c], Luigi Brambilla[e], Giuseppe Zerbi[e]

a)_Istituto per la Conservazione e la Valorizzazione dei Beni Culturali, CNR, Via Cozzi 53, 20125 Milano, Italy – b) DISAT, Università di Milano Bicocca, Milan, Italy; c) Dipartimento di Scienze della Terra, Università degli Studi di Milano, Via Botticelli 23, I-20133 Milano, Italy – d) Istituto di Cristallografia, CNR, Via G. Amendola 122/o, Bari, Italy – e) Dipartimento Chimica, Materiali e Ingegneria Chimica ''Giulio Natta'', Politecnico di Milano, Piazza Leonardo da Vinci 32, 20133 Milano, Italy

Abstract

Calcium oxalate is found in nature in three different crystalline states determined by the number of H_2Oin the unit formula (whewellite $CaC_2O_4H_2O$, COM; weddellite $CaC_2O_4(2+x)H_2O$, COD and caoxite$CaC_2O_43H_2O$, COT). The properties of these materials are relevant in the field of biomedicine, cultural heritage and mineralogy. In two previous papers, we have used X-ray diffraction and vibrational spectroscopy (infrared and Raman) to derive information on crystal and molecular structures of COM and COD. In this paper, we complete the synthesis and analysis on the third form, COT, and present a comparative study of the data collected from the three crystalline states. The experiments clearly highlighted role played by the H_2O molecules linked within the structure by different kinds of hydrogen bonds. The vibrational assignment of the infrared and Raman bands are critically proposed. The fact relevant for the work in biomedicine, cultural heritage and crystallography is that a simple examination of the spectra allows quickly to determine the chemical nature of the material in an unknown sample even in a minute quantity or in awkward experimental conditions

Keywords:Calcium oxalate trihydrate; Synchrotron X-ray diffraction; Caoxite synthesis; Raman spectroscopy; Infrared spectroscopy

Introduction

Calcium oxalate in the three different, and known, crystallographic forms (whewellite $CaC_2O_4H_2O$, COM; weddelliteCaC$_2O_4$ $(2+x)H_2O$, COD and caoxite $CaC_2O_43H_2O$, COT) shows properties which turn out to be of great interest in various fields of material science, namely biomedicine, mineralogy and cultural heritage. The characterization of these materials is essential also for the benefit of a quick analytical recognition, but so far it is not so easy to be carried out with physico-chemical or chemical techniques. While the structure and spectroscopic properties of COM and COD have been already matter of our previous works [1,2], in this paper we focus on caoxite. Here we describe first a new way to synthesize caoxite; the structure of the tiny single crystals obtained is studied by X-ray diffraction from a synchrotron source. Then we analyse the recorded infrared and Raman spectra. To the best of our knowledge, the Raman spectra are here reported and discussed for the first time. Our aim is first to revise the crystallographic data and secondly to rationalize the infrared and Raman spectra in the light of a comparative analysis of the spectra of the three forms. The outcome of this work is to provide first information of the structure and behavior of H_2O molecules which surround the oxalate ion in the crystal. A second useful consequence of our study is that we offer a comparison of the infrared and Raman spectra of the three forms which offers a direct way to immediately identify from the spectra the chemical nature of the material in a given sample. Caoxite is the triclinic tri-hydrated form of calcium oxalate found for the first time in 1997 as natural species in the Cerchiara mine, northern Apennines, Italy [3], even though the synthetic form was already known several years before [4]. Due to its thermodynamical instability, COT is less common than COM (monoclinic), the most table form, and then COD (tetragonal). COM and COD are major constituents of human urinary stones [5]and are found also in many organisms such as fungi, lichens, plants [6–8]and in rock weathering processes by lichens[9]. COT has been rarely found in urine and in kidney stones but it is considered as a possible precursor in their formation [10]. This justifies the fact that the few papers available in the literature on COT are found in the field of human pathology and they are devoted to the study of its crystallization mechanism in order to prevent kidney stone formation. In particular, the parameters that mainly influence the crystallization of COT and the crystal morphology in different precipitation conditions have been investigated [11–13].In the cultural heritage field, COM and COD play a relevant role since they are the main components of a particular kind of film found on the surface of many works of art[14]. Moreover, they occur also in a

conservation treatment for carbonatic substrates [15]used for some years on sculptures, mural façades, fresco paintings and mosaics to preserve the surfaces of their carbonatic substrates. The aqueous ammonium oxalate solution induces the transformation of part of calcium carbonate of the substrate to calcium oxalate (mainly COM) resulting in a better resistance to decay phenomena. Recently, in order to obtain a more homogeneous and deeper diffusion of the treatment into the decayed materials, additional experiments have been carried out to find new mechanisms of calcium oxalate crystallization in the carbonatic substrates. One of the most recent method, still under investigation, suggests the use of diethyloxalate[$(C_2H_5)_2C_2O_4$] which during the hydrolysis transforms calcium carbonate into calcium oxalate[16]. Diethyloxalate should achieve better diffusion because, in neutral conditions, duringthe hydrolysis the molecule should avoid the ionic interaction during its penetration. The reaction between diethyloxalate and calcite produces COM, COD and an unexpected relevant amount of COT [16], never detected during the studies of the ammonium oxalate treatment. The occurrence of COT is in agreement with the experimental finding of Echigo et al. [17],who obtained the crystallization of COT by the reaction of a similar molecule, dimethyloxalate [$(CH_3)_2C_2O_4$],with anhydrous calcium chloride ($CaCl_2$) at room temperature(23°C).The crystallization of COT into the treated carbonatic substrates the main proof of the reaction between diethyloxalate and the decayed stones, thus its identification is essential to monitor the treatment and define its efficacy. Up to now, the only analytical methods used to identify COT are X-ray diffraction (XRD)[3,10–13,17,18], Scanning Electron Microscopy (SEM)[10–13,19] and Fourier Transform Infrared Spectroscopy (FTIR)[10,17,20]. These studies provide information on the crystallographic structure of COT, the morphology of the crystals and the vibrations of the molecule. It has been recently shown that one of the most relevant technological advances to assess the diffusion of a product inside a substrate is Raman [21]. This technique allows mapping the strongest Raman lines of the starting materials and/or of the newly formed phases from the surface to the inner domains of the sample. To the best of our knowledge, no Raman spectra of COT are available in the literature, most likely because of the paucity of the material available. This fact increases the difficulty of develop-ing procedures for an easy and rapid identification of COT.

Experimental methods

In previous works, several approaches were used in order to obtain the three different calcium oxalate phases, even though the factors that influence their formation are not fully understood [18,22,23]. In this work, COT is obtained from the reaction between an aqueous solution of diethyl oxalate and calcite crystals. The reaction mechanism involves the slow hydrolysis of diethyl oxalate in water to form oxalic acid, which reacts with the calcite crystals producing calcium oxalate crystals [16]. The organic oxalic esters have already been proposed to produce oxalates minerals [24]. A 3% by volume aqueous solution of diethyl oxalate has been pre-pared and added to a stoichiometric amount of calcite crystals, obtained by grinding calcareous stone fragments. After grinding, the dimensions of calcite crystals were homogenized by sieving the calcite powders using a 32–80lm steel sieve; the sieving procedure is useful to simplify the microscope observation of the produced oxalate crystals. The calcite crystals immersed in the diethyloxalate solution were put in a sealed flask for 7 days, stored at room temperature and manually slightly stirred once a day. The reaction time was chosen taking in account the hydrolysis time of diethyl oxalate in water [16]. After the reaction, the solid phases were separated from the reaction solution by filtering. Since COT is the rarest and unstable form of hydrate calcium oxalate, the reproducibility of the proposed reaction procedure is affected by several factors such as temperature, reagent morphology and calcite crystals purity. In particular, the same reaction procedure has been performed using $CaCO_3$ Sigma Aldrich powder as solid reagent for the formation of calcium oxalate, instead of the stone-grinded calcite crystals. In the X-ray diffraction pattern of the second reaction products, COT was not detected. Several crystals were analysed on polarizing microscope and by X-ray diffraction in order to select a series of COT single crystals. In some cases, the crystals selection was very difficult due to the high degree of aggregation. The majority of COT crystals were found affected by inclusions or crystallographic defects. One crystal (0.085 x 0.065 x 0.015 mm), free of defects under the polarized microscope and with an apparently good diffraction pattern, was selected in order to collected X-ray intensity data, Raman and IR spectra-ray intensity data were first collected at room-T using a Xcalibur Oxford Diffraction diffractometer, equipped with a CCD detector and operating at 50 kV and 40 mA with monochromatized MoKa radiation. A combination of omega/phi scans, with 1°step and up to 30 s exposure time per frame, was chosen to maximize the redundancy and data coverage. The diffraction pattern was successfully indexed with the unit-cell of caoxite previously reported by Basso et al. [3]. However, the Bragg reflections were significantly weak in intensity, leading to a low number of observed reflections with $F_o > 4r(F_o)$. Using

the same crystal, a further diffraction experiment was then performed at the ID09A beamline, at the European Synchrotron Radiation Facility (ESRF), Grenoble, France, using the standard setup for single-crystal diffraction experiments [25]. A parallel monochromatic beam (E=30 kEv, lambda = 0.414601 Å) was used. The beam was vertically focused by a spherical mirror and horizontally by a bent silicon-(111) monochromator, in order to have a beam-size at the sample of 30x30 micrometers^2. The diffraction pattern was collected by a MAR555 flat panel detector. The data collection strategy consisted in a rotation of the crystal about the vertical omega-axis, within the range -45°<omega<+45°, with 1°stepscan and 1 s of exposure time per frame (Table 1). The diffraction pattern was successfully indexed with a triclinic unit-cell with a= 6.1097(13) Å, b= 7.1642(10) Å, c= 8.4422(17) Å, alpha = 76.43(1)°, beta = 70.19(2)°, gamma = 70.91(2)°, and V= 325.3(1) Å^3(Table 1). Intensity data were then integrated and corrected for Lorentz-polarization effects using the Crysalis software package [26]. A summary of the details pertaining to the X-ray diffraction experiment is given in Table 1. The X-ray structure refinement was then performed using theSHELXL-97 software [27–28]. Neutral scattering factors for Ca, C, O, and H have been taken from the International Tables for Crystallography Vol. C [29]. The atomic site positions reported by Basso et al. [3] have been used as starting structure model for the first refinement cycles. The first cycles have been performed with the atomic displacement parameters modeled as isotropic. The convergence was rapidly achieved. Further cycles have been performed with anisotropic displacements of Ca, C and O sites. H site positions were fixed to the values reported by Basso et al. [3]and not refined; their displacement regime was modeled with one isotropic parameter (Table 2). With such a configuration, the convergence was achieved and the shifts in all the refined parameters were less than their e.s.d. values, the variance–covariance matrix showed no significant correlations, and the residuals in the difference-Fourier synthesis of the electron density were < ± 1.1 e-/Å^3(Table 1). We obtained a final R_1= 0.111 for 841 reflections with F_o>4sigma(F_o) and 93 refined parameters (Table 1). Site coordinates, occupancy factors, displacement parameters, and relevant bond lengths and angles are given in Table 2. Raman spectroscopy analysis were carried out with a Senterra dispersivel-Raman spectrometer (Bruker) using 785 nm (NIR Diodes) and 532 nm (Nd:YAG laser) laser sources. The instrument was equipped with a Peltier cooled CCD detector (1024 x 256 pixels; -70°C) and coupled to an Olympus BX51 microscope. All spectra were collected through 20x and 50x objectives, that focuses the laser in a spot size of 5–3 micrometers approximately. The power at the sample and the exposure time ranged between 50 and100 mW and 100–200 s, respectively. The spectral resolution was about 3 cm-1 (1200 grooves/mm grating). Fourier transform infrared spectroscopy (FTIR) analyses were performed in the range 4000–650 cm-^{1} by a Thermo NicoletNexus spectrophotometer equipped with an Thermo Continuum microscope with a mercury cadmium telluride detector (MCT/A) cooled with liquid nitrogen. Measurements were carried out with the microscope in transmission mode pressing a single crystal of COT in a diamond anvil cell (sampling area 50 x 50 micrometers). Spectra were acquired with a resolution of 4 cm^{-1} by recording a total of 128 scans. A JEOL 5910LV Scanning Electron Microscope (SEM) was used in order to observe the synthesized COT crystals. The accelerating voltage was 20 kV and the specimen chamber was maintained in low vacuum modality (28 Pa).

Results and discussion

The mineralogical analysis of the calcareous stone used for COT synthesis, by X-ray powder diffraction, shows the presence of calcite ($CaCO_3$) as dominant phase and dolomite ($MgCa(CO_3)_2$) as secondary carbonate mineral (Fig. 1a). The crystals obtained in this study were observed by optical microscope and analysed by X-ray diffraction confirming the presence of all the three calcium oxalate phases (i.e., COM, COD, COT)(Fig. 1b). Due to the high degree of aggregation, single crystals were firstly separated from the crystalline aggregate (Fig. 2a) in order to better observe the morphologies that are consistent with the reported boat/coffin[11] or elongated hexagonal [10] COM crystals, as well as with the well-known bipyramidal crystals of COD[11,23](Fig. 2b). Residual calcite crystals were easily recognizable due to their opacity, while calcium oxalate phases have high transparency. The size of the crystals is extremely variable, from a few to a few hundreds micrometres; due to their high transparency and small thickness (2–3 micrometres), it is possible to observe crystals morphology also when they are overlapped (Fig. 2d). COT crystals were selected and observed in more detail by SEM. Fig. 3 shows representative SEM micrographs of the main COT morphologies obtained in this study; the different sizes and morphology makes difficult to distinguish the crystals of COT among the products The most common morphology is the elongated sword-like[10](Fig. 3a); other crystal exhibit an hexagonal squat shape (Fig. 3d).The observation of ‘‘free’’ single crystals of COT is quite difficult due to the presence of COD and COM on its surface or leaned to COT (Fig. 3c). The crystals are subjected to high decay under the

electron beam: after a few minutes, detachments and fractures are visible (Fig. 3b), confirming the high instability of this crystalline compound. The structure refinement based on the single-crystal synchrotron intensity data confirms that the material under investigation is COT, according to the experimental findings of Basso et al.[3]. The quality of the synthetic crystals, based on the optical observation and diffraction data, appears to be lower than the natural crystals. On the other hand, natural crystals are extremely rare, and we were not able to find any natural COT crystal for our experiments (i.e., all the crystals labelled as caoxite from museums or private collections that we analysed were actually not COT, but other Ca-oxalates). The building-block unit of the COT structure is shown in Fig. 4. It consists of two edge-sharing Ca-polyhedra, which are connected to other units through oxalate groups, in azig–zag fashion as shown in Fig. 4. Irregular sub-nanocavities occur in the structure of COT (Fig. 5). The Ca-polyhedron is significantly distorted. Its coordination number is CN = 8, represented by 4 oxygen atoms of the oxalate groups (i.e., O1, O2, O3and O42,Table 2) and by 3 H_2O molecules (i.e., OW1, OW2and OW3,Table 2)(Figs. 5 and 6). The distortion of the Ca-polyhedron can be described on the basis of the $D(Ca\text{-}O)_{max}$ (i.e., the difference between the longest and the shortest intra-polyhedral bond distance). The $D(Ca\text{-}O)_{max}$ deduced on the basis of the data reported by Basso et al.[1]is ca.0.13 Å, which is virtually identical to the value obtained on the basis of our experimental finding (i.e., ca. 0.13 Å, Table 2). A similar consistency is found for the geometrical configuration of the two independent oxalate groups: C1–O1 = 1.243 and C1–O2 = 1.253, C2–O3 = 1.251and C2–O4 = 1.259 Å were reported by Basso et al. [3]; C1–O1 = 1.245(7) and C1–O2 = 1.250(7), C2–O3 = 1.252(6) and C2–O4 = 1.259(7) Å obtained in this study (Table 2). A complex H-bonding network occurs in COT structure. At least five different H-bonds are energetically favourable: OW1-H5…O3, OW1-H4…O2, OW2-H2…O1, OW3-H6…OW1, and OW3-H3…OW2 (Fig. 6,Table 2). The two H-bonds withH_2O oxygen atoms as acceptors (i.e., OW1 and OW2, Table 2) are weaker than the further three with acceptors belonging to the oxalate groups (i.e., O1, O2 and O3,Table 2). TheO4 site appears not to be involved in the H-bonding scheme. O4–O4 is the edge shared by two adjacent Ca-polyhedra, thus each O4 site is bonded to two Ca sites and one C site, whereas O1, O2 and O3 are all bonded to one Ca and one C site (Figs. 5and 6). The acquisition of the infrared and Raman spectra of the three forms of crystalline calcium oxalate allows to carry out an overall comparative analysis of the vibrational properties of these systems. In this case, the analysis was favoured by the availability of detailed studies of the crystal structure of these systems previously carried out with X-ray diffraction [17,30]. The first relevant observation is that the three crystalline forms consist only of a different organization of H_2O molecules which are clustered around the $C_2O_4Ca_2$basic unit, forming different kinds of networks of hydrogen bonds. The positions of H_2O molecules are well determined for the mono-hydrate (whewellite) and the tri-hydrate forms, while in the di-hydrated form (weddellite) one of the H_2O molecules has been found to be highly disordered along the channel of the crystal structure. We can easily simplify the interpretation of the vibrational infrared and Raman spectra of the three systems by considering that the unit cell of each of the structures is built by two entities, namely one unit $C_2O_4Ca_2$surrounded by a network of H_2O molecules which forms hydrogen bonds both with the central unit and among themselves. We can consider the $C_2O_4Ca_2$unit as acted upon by an inter-molecular effective mean potential field much weaker than the intra-oxalate potential where covalent, or relatively strong electrostatic forces, are active in keeping the C, O and Ca atoms together. In terms of vibrational coupling, the perturbation by the surrounding medium on the carboxylate unit can be assumed to be small and we can discuss the dynamics of the two entities as separated. The decision to proceed in the analysis of the spectrum by considering the vibration of the oxalate group as separated from that of the surrounding net implies that we forcefully neglect the vibrations of the lattice which are observed in the lowest frequency range of the spectrum (where it is likely that also the lowest frequency deformation modes may occur). We then first proceed on the vibrational analysis of the $C_2O_4Ca_2$unit which is assumed to have the average structure shown in Fig. 7. Such a structure, of the type X_2Y_4, is commonly found in many other molecules and its vibrations have been treated as text-book case. For sake of clarity and consistency, we refer to the numbering, symmetry and approximate shape of the normal modes as given by Herzberg.[31]The system considered belongs to the point group D_{2h}; the structure of the irreducible representation and the corresponding selection rules for the 3 N-6 = 12 normal modes are the following:

$$\Gamma_{vib} = 3A_g(R,pol) + B_{2g}(R,depol) + 2B_{3g}(R,depol) + A_u(inactive) + 2B_{1u}(IR,\mu_z) + 2B_{2u}(IR,\mu_y) + B_{3u}(IR,\mu_x)$$

In the expression of the irreducible representation, we have indicated the degree of depolarization of the Raman lines as well as the direction of the changes of the dipole moments for the nor-mal modes of a molecule necessarily considered in vacuo. In the prediction of the Raman spectra generally one expects that the totally symmetric modes (A_g) are much stronger than the modes with species B_{2g} and B_{3g}, which may turn out to be extremely weak and

sometimes cannot be observed. A final remark concerns the fact that we expect only one infrared-active normal mode with changes of dipole moment out of the plane of the molecular unit, generally associated with an absorption band of sizeable intensity in the lower frequency part of the spectrum. The vibrations of the second entity, i.e. the motions of the hydrogen-bonded ''nets'' different for the three compounds, will be discussed below. At this point of our comparative study, we must be aware of the fact that the effective mean potential field, envisaged above, may (weakly) act upon the central unit in different ways for the three systems. The perturbations may induce (i) small frequency shifts, (ii) changes of relative intensities and (iii) breakdown of the strict symmetry selection rules worked out for the X_2Y_4 with the consequent weak activation of Raman transitions in IR and viceversa, thus removing the strict rule of IR/Raman non coincidence expected for centrosymmetric systems. When Wilson's type internal displacement coordinates are used in the description of the normal modes [32], the transformation from internal to symmetry coordinates as given in Fig. 7 provides a very clear description of the approximated modes expected for the oxalate ion. We shall proceed in the vibrational assignments of the modes as described in the following by the symmetry coordinates depicted in Fig. 7. The symmetry species are referred to the modes of the ideal ''average'' model. The choice of the totally symmetric modes is made easier by the expected strength of the corresponding Raman lines which are located at 1472, 912 and 867 cm-1 (Fig. 8 left); they can be assigned respectively to ν_1, ν_2, ν_3. While ν_1 is clearly a totally symmetric CO stretching, μ_2 and μ_3 must be associated to the in-phase symmetric bending of the OCO group and the stretching of the C–C bond. Evidently, the mechanical coupling (allowed by symmetry) of μ_2 and μ_3 modes must be strong and any distinction is necessarily arbitrary; because of this mechanical coupling, one of the two modes can borrow the intensity from the other. The Raman spectrum in the range 1750–1300 cm-1 shows also several weak lines whose origin does not have an unequivocal assignment, with the exception of the peak near 1668 cm^{-1} which will be discussed below. The other lines may originate from combinations and/or overtone transitions or from the activation of infrared bands caused by the lower of the symmetry originated from the surrounding net of hydrogen bonds. The assignment is not essential for the aim of this work. The infrared active transitions for the oxalate group are observed at 1624 cm-1 and 1327 cm-1 (ν_{11} and ν_9 respectively) and are assigned to the infrared active CO stretching (Fig. 8 right). The in-plane OCO bending is assigned to the band at 783 cm-1 (ν_{12}). The assignment of the OCO in phase rocking ν_6 (Raman) and out of phase ν_{10} (IR) is not straightforward; we can tentatively assign the Raman line at 507 cm-1 while we have no data available for the infrared. Problems arise in the assignment of both infrared and Raman spectra to be associated to the normal modes of H_2O molecules, which govern the complex hydrogen-bonded net surrounding the oxalate ions as previously discussed. A comparison of the spectra of the three modifications of calcium oxalates (COM, COD and COT–Fig. 9) allows to draw some analogies regarding the vibrations of H_2O molecules. Let us first consider the OH stretching range (3700–2700 cm-1), where very broad bands are observed for caoxite and weddellite while a finer structure is found for whewellite. As already discussed [1], the breath of the absorption has to be ascribed to a structural disorder of the position of H_2O molecules in weddellite, while the existence of a single H_2O molecule in whewellite allows the formation of more ordered hydrogen-bonded net. An attempt to rationalize the IR spectrum of caoxite in this frequency range suggests that the spectrum can be divided in two parts: abroad one centered near 3220 cm-1 and a second one with two broad peaks near 3430 and 3530 cm-1 (Fig. 9 right). It is known that the stronger is the hydrogen bond the lower is the OH stretching frequency; it follows that from the spectrum we may envisage that at least two types of hydrogen bonds with different strengths exist in the net of caoxite. This is in agreement with the observation derived from the X-ray structure refinement of this study, which provides evidence of at least two types of hydrogen bonds with different lengths (strengths).The distinction of the two types of H_2O molecules is not indicated by the absorption of OH bending located at 1668 cm^{-1}, broad shoulder in the IR and very weak in the Raman. The search of the librational motions of H_2O molecules forces us to assign this mode to the yet unexplained line observed at 582 cm-1 intrinsically weak and broad in the Raman spectrum (for technical reasons ,we could not collect the infrared spectrum below 700 cm^{-1}). The same weak line is observed for weddellite (broad) and for whewellite (sharp). In Table 3 the IR and Raman bands of the three calcium oxalates have been reported.

Conclusions

This is the first comparative analysis of the IR and Raman spectra of whewellite, weddellite and caoxite, which provides a quick and reliable identification protocol among Ca-oxalates. In this work, a new synthesis procedure of COT is described as valid alternative to the others proposed in the literature. However, the synthesis is difficult and it

is hard to obtain single crystals for structural determination. The crystalline structure of COT obtained in this study is virtually identical to that reported by Basso et al.[3]and Deganello et al.[18]. To the best of our knowledge, the Raman spectrum of COT is reported in this paper for the first time. Both FTIR and Raman spectra of COT have been here described. A comparison of the vibrational spectra of the three forms of calcium oxalates clearly shows that the perturbation of the oxalate group by the net of hydrogen-bonded H_2O molecules is negligible. The complex H-bonding network of COT has been discussed, bridging crystallographic and spectroscopic data, and showing a complex net of H-bonding interactions. The infrared and Raman active transition frequencies appear being can be correlated with the lengths (strengths) of the hydrogen bonds.

Acknowledgment

The authors thank ESRF – Grenoble for the allocation of beamtime.

References

[1]C. Conti, L. Brambilla, C. Colombo, D. Dellasega, G.D. Gatta, M. Realini, G. Zerbi,Stability and transformation mechanism of weddellite nanocrystals studied byX-ray diffraction and infrared spectroscopy, Phys. Chem. Chem. Phys. 12(2010) 14560–14566.[2]C. Conti, M. Casati, C. Colombo, M. Realini, L. Brambilla, G. Zerbi, Phasetransformation of calcium oxalate dihydrate–monohydrate: effects of relativehumidity and new spectroscopic data, Spectrochim. Acta A 128 (2014) 413–419.[3]R. Basso, G. Lucchetti, L. Zefiro, A. Palenzona, Caoxite, $Ca(H_2O)_3(C_2O_4)$, a newmineral from Cerchiara mine, northern Apennines, Italy, Neues Jahrbuch fürMineralogie Abhandlungen 2 (1997) 84–96.[4]G. Hammarsten, Comptes-Rendus Laboratoire Carlsberg, Copenhague 17(1929).[5]M. Daudon, D. Bazin, G. Andre´, P. Jungers, A. Cousson, P. Chevallier, E. Veron, G.Matzen, Examination of whewellite kidney stones by scanning electronmicroscopy and powder neutron diffraction techniques, J. Appl. Cryst. 42(2009) 109–115.[6]V.R. Franceschi, H.T. Horner, Calcium oxalate crystals in plants, Botanical Rev.46 (1980) 361–427.[7]M. Guggiari, R. Bloque, M. Aragno, E. Verrecchia, D. Job, P. Junier, Experimentalcalcium-oxalate crystal production and dissolution by selected wood-rot fungi,Int. Biodeterior. Biodegr. 65 (2011) 803–809.[8]P. Giordani, P. Modenesi, M. Tretiach, Determinant factors for the formation ofthe calcium oxalate minerals, weddellite and whewellite, on the surface offoliose lichens, Lichenologist 35 (2003) 255–270.[9]P. Adamo, P. Violante, Weathering of rocks and neogenesis of mineralsassociated with lichen activity, Appl. Clay Sci. 16 (2000) 229–256.[10]J.M. Ouyang, H. Zheng, S.P. Deng, Simultaneous formation of calcium oxalate(mono-, di-, and trihydrate) induced by potassium tartrate in gelatinoussystem, J. Cryst. Growth 293 (2006) 118–123.[11]C.P. East, A.D. Wallace, A. Al-Hamzad, W.O.O. Doherty, C.M. Fellows, Effect ofpoly(acrylic acid) molecular mass and end-group functionality on calciumoxalate crystal morphology and growth, J. Appl. Polym. Sci. 115 (2010) 2127–2135.[12]R.C. Walton, J.P. Kavanagh, B.R. Heywood, P.N. Rao, Calcium oxalates grown inhuman urine under different batch conditions, J. Cryst. Growth 284 (2005)517–529.[13]M. Donnet, N. Jongen, J. Lemaitre, P. Bowen, New morphology of calciumoxalate trihydrate precipitated in a segmented flow tubular reactor, J. Mater.Sci. Lett. 19 (2000) 749–750.[14]L. Rampazzi, A. Andreotti, I. Bonaduce, M.P. Colombini, C. Colombo, L. Toniolo,Analytical investigation of calcium oxalate films on marble monuments,Talanta 63 (2004) 967–977.[15]B. Doherty, M. Pamplona, R. Selvaggi, C. Miliani, M. Matteini, A. Sgamellotti, B.Brunetti, Efficiency and resistance of the artificial oxalate protection treatmenton marble against chemical weathering, Appl. Surf. Sci. 253 (2007) 4477–4484.[16]C. Conti, I. Aliatis, M. Casati, C. Colombo, M. Matteini, R. Negrotti, M. Realini, G.Zerbi, Diethyl oxalate as a new potential conservation product for decayedcarbonatic substrates, J. Cult. Herit.15 (2013) 336–338.[17]T. Echigo, M. Kimata, A. Kyono, M. Shimizu, T. Hatta, Re-investigation of thecrystal structure of whewellite $[Ca(C_2O_4)H_2O]$ and the dehydrationmechanism of caoxite $[Ca(C_2O_4)3H_2O]$, Miner. Mag. 69 (2005) 77–88.[18]S. Deganello, A.R. Kampf, P.B. Moore, The crystal structure of calcium oxalatetrihydrate; $Ca(H_2O)_3(C_2O_4)$, Am. Miner. 66 (1981) 859–865.[19]F. Grases, A. Millan, A. Conte, Production of calcium oxalate monohydrate,dihydrate and trihydrate, Urol. Res. 18 (1990) 17–20.[20]W. Heijnen, W. Jellinghaus, W.E. Klee, Calcium oxalate trihydrate in urinarycalculi, Urol. Res. 13 (1985) 281–283.[21]C. Conti, C. Colombo, M. Matteini, M. Realini, G. Zerbi, Micro-Raman mappingon polished cross sections: a tool to define the penetration depth ofconservation treatment on cultural heritage, J. Raman Spectrosc.41 (2010)1254–1260.[22]L. Brecevic, D. Kralj, J. Garside, Factors influencing the distribution of hydratesin calcium oxalate precipitation, J. Cryst. Growth 970 (1989) 460–468. [23]B. Bernard-Michel, M. Pons, H. Vivier, S. Rohani, The study of calcium oxalateprecipitation using image analysis, Chem. Eng. J.75 (1999) 93–103.[24]A.M. Feibush, K. Rowley, L. Gordon, Coprecipitation in some binary systems ofrare Earth oxalates, Anal. Chem. 30 (1958) 1605–1609.[25]M. Merlini, M. Hanfland, Single-crystal diffraction at megabar conditions bysynchrotron radiation, High Pressure Res. 33 (2013) 511–522.[26] Agilent, Xcalibur CCD system, Crysalis software system, 2012.[27]G.M. Sheldrick, SHELX-97 – A Program for Crystal Structure Refinement,University of Göttingen, Göttingen, 1997.[28] G.M. Sheldrick, A short history of SHELX. Acta Crystallographica, A64, 112–122.[29]A.J.C. Wilson, E. Prince, International Tables for Crystallography, Vol. C,Mathematical, Physical and Chemical Tables, second ed., Kluwer, Dordrecht,1999.[30]V. Tazzoli, C. Domeneghetti, The crystal structures of whewellite andweddellite: re-examination and comparison, Am. Miner. 65 (1980) 327–334.[31] G. Herzberg, Molecular Spectra and Molecular Structure, Infrared and RamanSpectra of Polyatomic Molecules, Vol. 3, Van Nostrand Ed., New York, 1960.[32]E.B. Wilson, J.C. Decius, P.C. Cross, Molecular Vibrations, McGraw Hill Ed., NewYork, 1955.

Table 1
Details pertaining to the X-ray data collection and structure refinement of caoxite.

Crystal shape	Prismatic
Crystal size (mm)	0.085 × 0.065 × 0.015
Crystal color	Translucent white
Unit-cell constants	a = 6.1097(13) Å
	b = 7.1642(10) Å
	c = 8.4422(17) Å
	α = 76.43(1)°
	β = 70.19(2)°
	γ = 70.91(2)°
	V = 325.3(1) Å^3
Space group	$P\bar{1}$
Reference formula	$CaC_2O_4{\cdot}3H_2O$
Z	2
T (K)	298
Radiation (λ)	0.414601 Å
Diffractometer	ID09A beamline, ESRF
Data-collection method	ω-scan, 1°/frame, 1 s/frame
Max. 2θ (°)	34.6
	$-7 \leqslant h \leqslant 7$
	$-9 \leqslant k \leqslant 10$
	$-9 \leqslant l \leqslant 9$
No. measured reflections	1341
No. unique reflections	957
No. unique refl. with $F_o > 4\sigma(F_o)$	841
No. refined parameters	93
R_{int} (Friedel pairs)	0.0553
R_1 (F) with $F_o > 4\sigma(F_o)$	0.1119
R_1 (F) for all the unique refl.	0.1173
wR_2 (F^2)	0.1316
Weighting Scheme: a, b	0.01, 0
Residuals (e^-/Å^3, fm/Å^3)	+1.09/−0.83

Note: $R_{int} = \Sigma|F^2_{obs} - F^2_{obs}(mean)|/\Sigma[F^2_{obs}]$; $R_1 = \Sigma(|F_{obs}| - |F_{calc}|)/\Sigma|F_{obs}|$; $wR_2 = [\Sigma[w(F^2_{obs} - F^2_{calc})^2]/\Sigma[w(F^2_{obs})^2]]^{0.5}$, $w = 1/[\sigma^2(F_{obs}{}^2) + (a{*}P)^2 + b{*}P]$, $P = (\mathrm{Max}(F_{obs}{}^2, 0) + 2{*}F_{calc}{}^2)/3$.

Table 2
Fractional site coordinates, site occupancy factor (*s.o.f*), displacement parameters (Å^2) and relevant bond distances (Å) and angles (°) of caoxite based on the X-ray structure refinement. The anisotropic displacement factor exponent takes the form: $-2\pi^2[(ha^*)^2U_{11} + \ldots + 2hka^*b^*U_{12}]$. U_{eq} is defined as one third of the trace of the orthogonalised U_{ij} tensor.

Site	s.o.f.	*x*	*Y*	*z*	U_{11}	U_{22}	U_{33}	U_{12}	U_{13}	U_{23}	U_{eq}/U_{iso}
Ca	Ca, 1.0	0.5925(3)	0.2807(2)	0.1924(2)	0.0311(9)	0.0468(8)	0.0167(10)	−0.0192(6)	0.0008(9)	0.0002(5)	0.0322(6)
C1	C, 1.0	0.4438(17)	0.5979(8)	0.4488(9)	0.051(5)	0.031(3)	0.037(5)	−0.011(3)	−0.010(6)	0.006(3)	0.042(2)
C2	C, 1.0	0.0739(13)	0.4320(11)	0.0571(12)	0.025(3)	0.057(4)	0.019(5)	−0.016(3)	0.010(5)	−0.008(4)	0.037(2)
O1	O, 1.0	0.4250(19)	0.5914(7)	0.3081(8)	0.106(7)	0.036(2)	0.033(4)	−0.011(3)	−0.029(6)	−0.004(2)	0.058(2)
O2	O, 1.0	0.6270(14)	0.2495(7)	0.4803(8)	0.079(5)	0.055(3)	0.025(4)	−0.025(3)	−0.012(5)	0.002(3)	0.053(2)
O3	O, 1.0	0.0027(12)	0.2837(10)	0.1422(10)	0.047(3)	0.079(3)	0.057(5)	−0.042(3)	−0.023(5)	0.034(4)	0.060(2)
O4	O, 1.0	0.2663(9)	0.4648(7)	0.0528(8)	0.033(3)	0.051(2)	0.026(4)	−0.023(2)	−0.003(4)	0.005(2)	0.037(1)
OW1	O, 1.0	0.2671(10)	0.1373(8)	0.3692(9)	0.044(3)	0.052(2)	0.049(5)	−0.021(2)	−0.013(5)	0.012(3)	0.050(2)
OW2	O, 1.0	0.3152(18)	0.8778(8)	0.0565(10)	0.101(6)	0.048(3)	0.044(5)	0.004(3)	−0.038(6)	−0.012(3)	0.065(2)
OW3	O, 1.0	0.2009(13)	0.0804(8)	0.7431(10)	0.053(4)	0.054(3)	0.041(5)	−0.005(3)	0.015(6)	−0.004(3)	0.060(2)
H1	H, 1.0	0.228	0.008	0.081							0.25(7)*
H2	H, 1.0	0.334	0.802	0.144							0.25(7)*
H3	H, 1.0	0.046	0.116	0.803							0.25(7)*
H4	H, 1.0	0.704	0.001	0.589							0.25(7)*
H5	H, 1.0	0.138	0.161	0.324							0.25(7)*
H6	H, 1.0	0.198	0.150	0.640							0.25(7)*
Ca -	O1	2.410(5)	OW1-H5	0.940(8)	OW3-H6	0.899(8)					
	O2	2.463(6)	OW1···O3	2.73(1)	OW3···OW1	2.99(1)					
	O3	2.403(7)	H5···O3	1.889(9)	H6···OW1	2.198(7)					
	O4	2.498(6)	OW1-H5 ···O3	147.3(5)	OW3-H6···OW1	146.5(6)					
	O4	2.530(6)									
	OW1	2.416(6)	OW1-H4	0.949(6)							
	OW3-H3	0.892(7)									
	OW2	2.433(7)	OW1···O2	2.73(2)	OW3···OW2	2.98(1)					
	OW3	2.500(7)	H4···O2	1.79(1)	H3···OW2	2.11(1)					
			OW1-H4 ···O2	168.4(4)	OW3-H3···OW2	165.0(6)					
C1 -	O1	1.244(10)									
	O2	1.250(8)	OW2-H2	0.826(7)							
C2 -	O3	1.252(11)	OW2···O1	2.682(9)							
	O4	1.260(9)	H2···O1	1.870(6)							
			OW2-H2 ···O1	167.2(5)							

Note: The e.s.*d*s of the O–H bond distances are likely underestimated as the site positions of the H1-6 sites were fixed to the values reported by Basso et al. [3] and not refined.
*Restrained to the same value.

Table 3
IR and Raman bands (in cm^{-1}) (532 nm laser excitation) for whewellite, weddellite and caoxite ("w" weak, "m" medium, "s" strong, "sh" shoulder, "br" broad). See text and Fig. 7 for band assignments.

IR			Raman		
Whewellite	Weddellite	Caoxite	Whewellite	Weddellite	Caoxite
3483 m	3469 b	3528 w-m	3486 w	3500–3200 br	3500–3200 br
3429 m		3427 w-m	3426 m		
3336 m		3222 w-m	3340 w		
3258 m			3256 w		
3058 m			3056 m		
			2972 w	2941 m	2941 m
			2919 w	2855 w	2882 w
1645 sh	1640–1638 s	1668 sh (H_2O)	1629 m s	1631 m s	1668 w br (H_2O)
1624–1622 s		1624 s			
			1490 vs	1476 vs	1472 vs
			1463 vs		
1384 w		1382 sh	1396 m s	1416 br	1418 br
1368 w					
1320–1316 s	1330–1327 s	1327 m	942 w br	911 s	912 s
			896 s		
950 w	917–915 w		863 m	870 m	867 m s
885 w					
783–781 m s	784–782 m br	783 w-m			
668 m	619 m br				
597 w			597 m s	597 w br	582 w br (H_2O)
517 m	515 m		522 m s		
			503 s	506 s	507 s

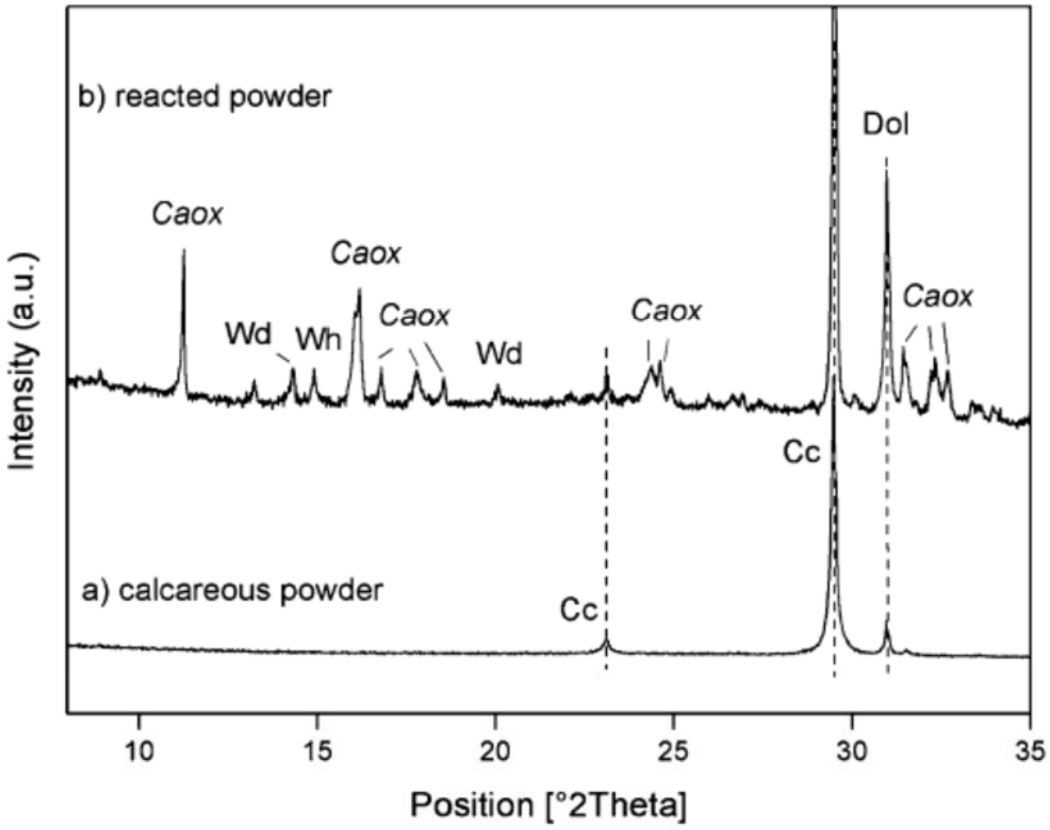

Fig. 1. XRD patterns of the carbonatic powder before (a) and after (b) the reaction with diethyl oxalate. Caox (caoxite), Wd (weddellite), Wh (whewellite), Dol (dolomite) and Cc (calcite).

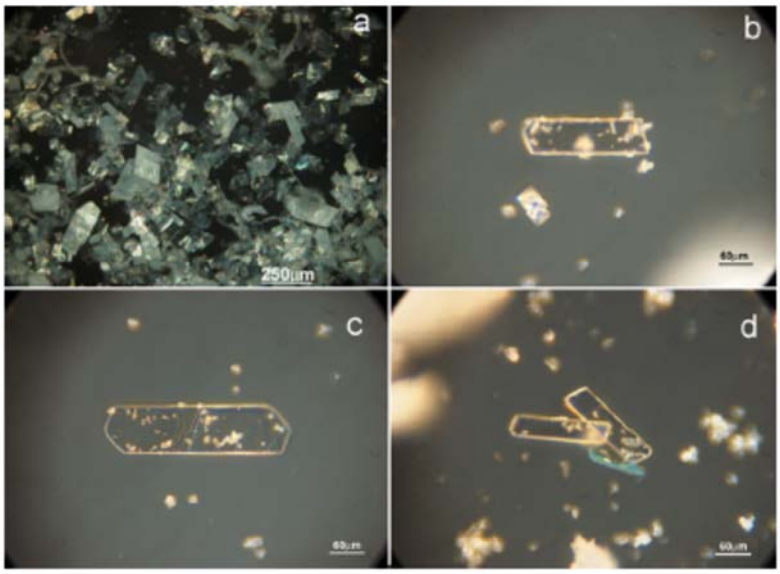

Fig. 2. Optical microscopy images of calcium oxalates crystallized after the reaction of carbonatic powder with diethyl oxalate. The crystalline aggregate (a) includes single crystal of COM (b), COD (b) and COT (c, d).

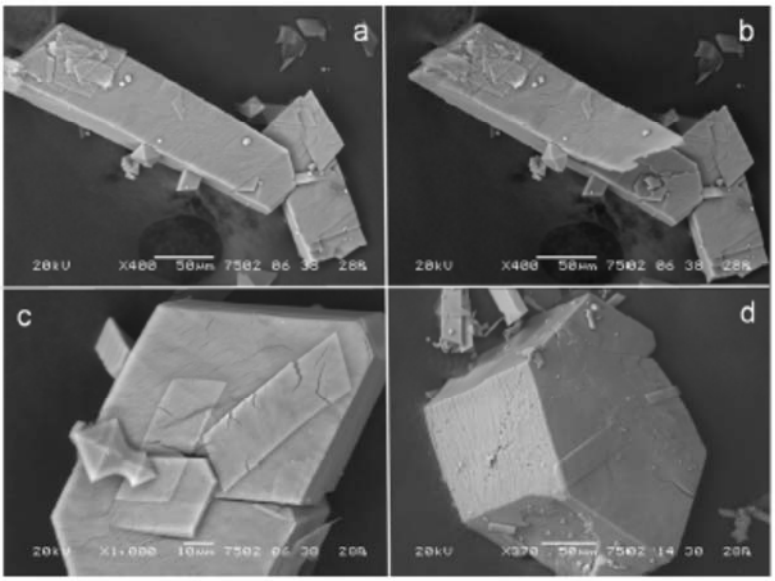

Fig. 3. SEM images of COT crystals with different morphologies: the elongated sword-like caoxite crystal before (a) and after (b) the decay under the electron beam; presence of bipyramidal COD and boat-coffin COM crystals on the surface of a COT crystal (c) and hexagonal squat shape of a COT crystal (d).

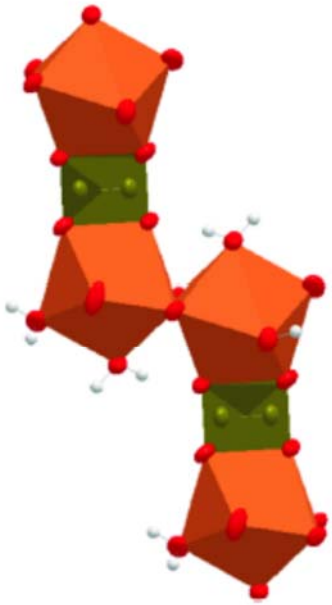

Fig. 4. Building block units of the COT structure: two edge-sharing Ca-polyhedra (in orange), which are connected to other units through oxalate groups (in green). (For interpretation of the references to color in this figure legend, the reader is referred to the web version of this article.)

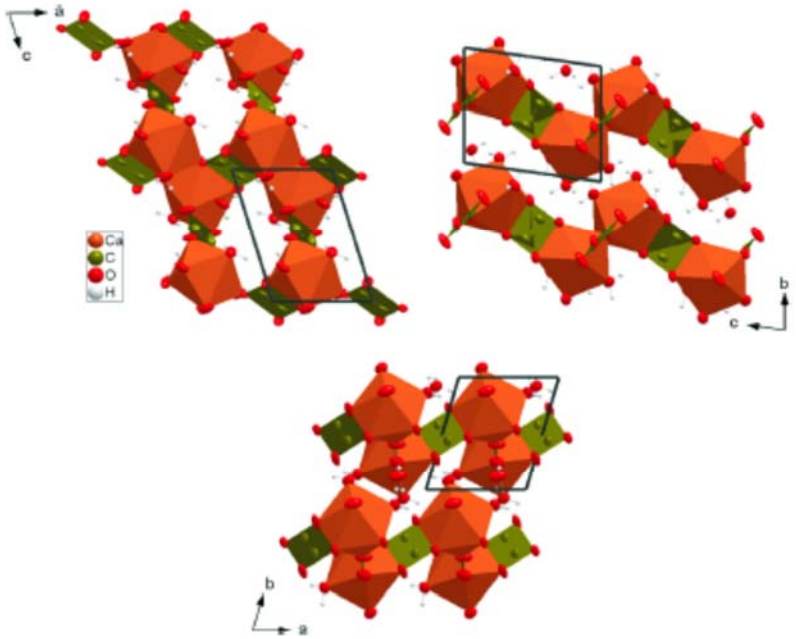

Fig. 5. Three views of the COT structure (*i.e.*, perpendicular to (010), (100) and (001)) based on the structure refinement of this study. Displacement parameters probability factor: 50%.

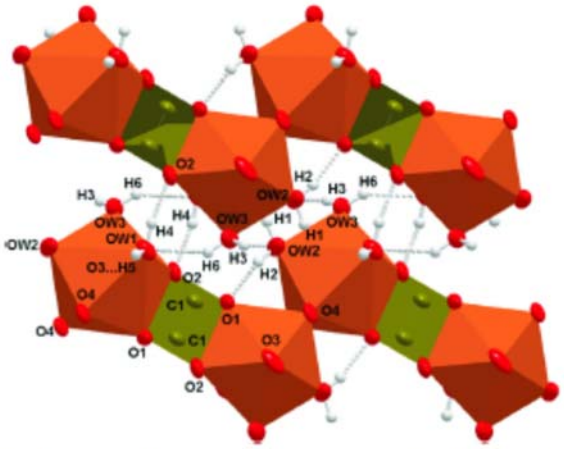

Fig. 6. The complex H-bonding network in COT structure. The OW1-H5···O3 bond is not shown in this view. Displacement parameters probability factor: 50%.

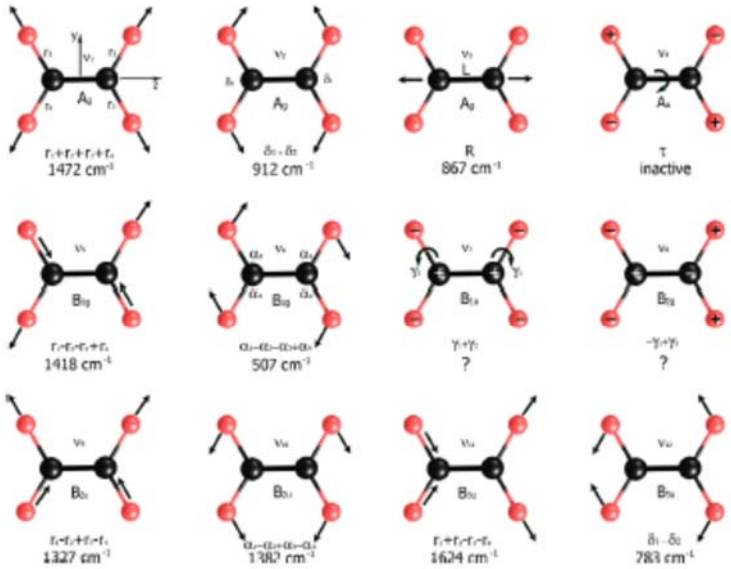

Fig. 7. Average geometry of the oxalate ion with the definition of the internal coordinates (R) used indicates that there is symmetry coordinates as linear combinations of R for an approximate description of the normal modes; vibrational assignment (the labeling follows those given by Herzberg[31]); ? indicates that there is no evidence supporting the choice of a given vibrational transition.

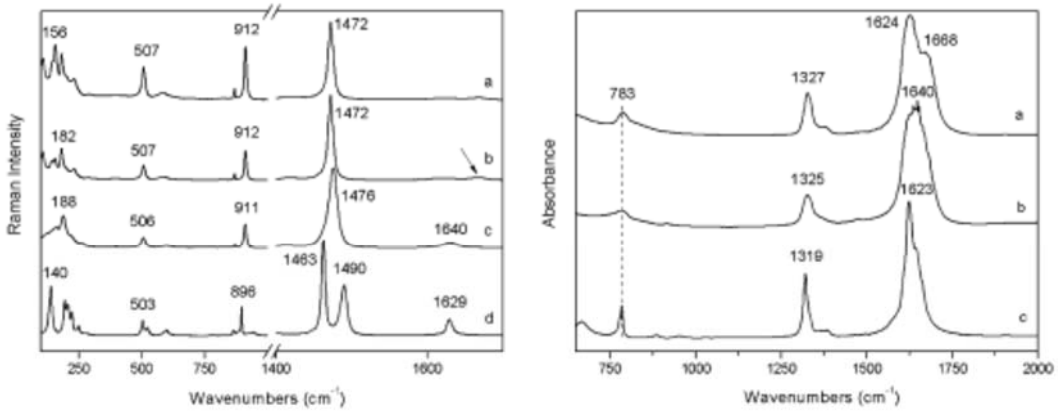

Fig. 8. Raman spectra of (a) COT (785 nm laser line), (b) COT (532 nm laser line), (c) COD (532 nm laser line), (d) COM (532 nm laser line) – *left*. FTIR spectra of (a) COT, (b) COD and (c) COM – *right*.

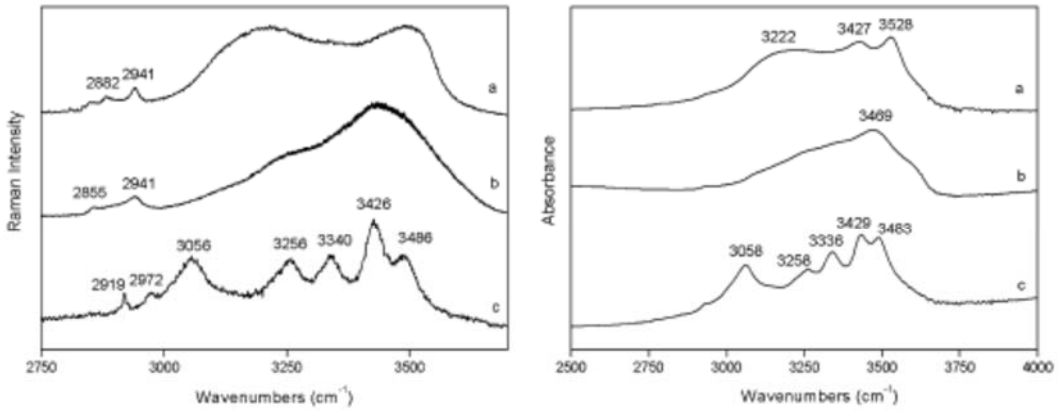

Fig. 9. 532 nm laser-source Raman (*left*) and FTIR (*right*) spectra in the OH stretching region of (a) COT, (b) COD and (c) COM.